A global multilayer cloud identification with POLDER/PARASOL

A Global Multilayer Cloud Identification with POLDER/*PARASOL*

M. DESMONS

Department of Meteorology, University of Reading, Reading, United Kingdom

N. FERLAY, F. PAROL, J. RIÉDI, AND F. THIEULEUX

Laboratoire d'Optique Atmosphérique, Université des Sciences et Technologies de Lille, Villeneuve d'Ascq, France

(Manuscript received 29 April 2016, in final form 6 January 2017)

ABSTRACT

The detection of multilayer cloud situations is important for satellite retrieval algorithms and for many climate-related applications. In this paper, the authors describe an algorithm based on the exploitation of the Polarization and Directionality of the Earth's Reflectance (POLDER) observations to identify monolayered and multilayered cloudy situations along with a confidence index. The authors' reference comes from the synergy of the active instruments of the A-Train satellite constellation. The algorithm is based upon a decision tree that uses a metric from information theory and a series of tests on POLDER level-2 products. The authors obtain a multilayer flag as the final result of a tree classification, which takes discrete values between 0 and 100. Values closest to 0 (100) indicate a higher confidence in the monolayer (multilayer) character. This indicator can be used as it is or with a threshold level that minimizes the risk of misclassification, as a binary index to distinguish between monolayer and multilayer clouds. For almost fully covered and optically thick enough cloud scenes, the risk of misclassification ranges from 29% to 34% over the period 2006–10, and the average confidences in the estimated monolayer and multilayer characters of the cloud scenes are 74.0% and 58.2%, respectively. With the binary distinction, POLDER provides a climatology of the mono–multilayer cloud character that exhibits some interesting features. Comparisons with the performance of the Moderate Resolution Imaging Spectroradiometer (MODIS) multilayer flag are given.

1. Introduction

Clouds are a key component of Earth's climate system. Their presence is the result of thermodynamic and microphysic processes in the atmosphere. Consequently, their structures can indicate various atmospheric states and meteorological events. For instance, frontal cloud systems indicate the encounter of different air masses, vertically large extended clouds are the sign of large available potential energy, and the base of warm clouds indicates their condensation level. In return, the effects of cloud cover on the climate is important. The radiative effects of clouds at the top of the atmosphere, as well as effects on the surface energy budgets, are significant and diverse. They also significantly affect the atmospheric circulation through the exchange of latent heat during their lifetime.

A global observation and description of clouds are necessary to understand and properly depict their overall and multiple effects. This is particularly true in the context of the climate change we are experiencing. Whether cloud covers of different cloud types or the partition of low-level versus high-level clouds—which have different and sometimes opposite radiative effects—will remain regionally or globally unchanged or will evolve is a crucial question. It is recognized as one of the major challenges in climate change predictions (Bony and Dufresne 2005; Andrews et al. 2012; Vial et al. 2013). Some recent studies argue that a consequence of climate change would likely be a change in the cloud vertical distribution (Chepfer et al. 2014).

One important and common feature of cloud covers is their multilayer character. A thin layer of high cloud above a lower one may affect significantly the vertical profile of net radiative fluxes (Christensen et al. 2013), and this top layer may skew the retrieval of cloud properties mainly based on the assumption of a single layer.

Corresponding author e-mail: N. Ferlay, nicolas.ferlay@univ-lille1.fr

DOI: 10.1175/JAMC-D-16-0159.1

Multilayer cloud cases have first been detected by surface observations (Hahn et al. 1990a,b; Warren et al. 2014) or in situ through the use of sounding balloons (Wang et al. 2000). The development of active remote sensing instruments has improved the identification of multilayered cloudy situations as well as the description of their properties (Mace et al. 2009; Yuan and Oreopoulos 2013). Satellite-based observations from passive sensors having a large field of view are adequate to infer cloud microphysical and bulk properties and study globally and statistically the interaction between radiation and clouds. The detection and characterization of multilayer cloud systems with passive remote sensing instruments remains, however, limited. Indeed, from space, for example, a high cloud layer can be optically thick and consequently overshadow a lower one. Reciprocally, in the presence of thick low clouds, high layers can be optically too thin to be detected by a passive remote sensing instrument. Last, the vertical distance between two cloud layers is sometimes too low for the scene to be identified as multilayered by a passive instrument. Given awareness of these difficulties, several methods have been proposed to detect multilayered cloudy situations with passive sensors.

Sheu et al. (1997) combine infrared and microwave measurements, as high clouds are practically transparent in the microwave domain but are much more opaque in the infrared domain. Baum et al. (1995) suggested a semiautomatic method based on multispectral and multiresolution measurements [multispectral, multiresolution (MSMR) method]. Jin and Rossow (1997) also use a multispectral method, based on the fact that when a low cloud is present under a thin and high cloud, cloud-top pressure determined by the CO_2 slicing method varies with the wavelength. This method makes it possible to detect a thin cloudy layer ($\tau \leq 1$) above a low layer, with both of them being separated by at least 100 hPa. A bispectral approach has been developed by Baum and Spinhirne (2000) and then by Nasiri and Baum (2004) in order to detect optically thin cirrus that overlap low-level liquid clouds when they are separated by at least 2 km. It exploits the fact that absorption by ice at 1.63 μm is very high relative to that of liquid water, such that reflectance at this wavelength stays the same when the cirrus optical thickness increases. In the meantime, the brightness temperature at 11 μm strongly depends on cirrus optical thickness. Pavolonis and Heidinger (2004) and Heidinger and Pavolonis (2005) combine visible and infrared measurements to detect cirrus ($0.5 < \tau < 4$) above low clouds ($\tau > 5$). Chang and Li (2005) compare cirrus optical thickness deduced from visible and infrared measurements. Wind et al. (2010) have elaborated an operational algorithm for the Moderate Resolution Imaging Spectroradiometer (MODIS) (Platnick et al. 2003; King et al. 2003) instrument, whose principal objective is the detection of multilayered cloudy situations, specifically optically thin ice clouds overlying lower-level water clouds. In this algorithm, the MODIS 0.94-μm water vapor band is used along with CO_2 bands to obtain two above-cloud precipitable water retrievals, the difference of which, in conjunction with additional tests, provides information on where multilayer clouds potentially exist. Joiner et al. (2010) combine information about cloud-top pressure deduced from thermal infrared and solar measurements in order to identify multilayered situations from vertically extended clouds. Yao et al. (2010) use cloud thermodynamic phase retrieved by the Polarization and Directionality of the Earth's Reflectance (POLDER) radiometer (Buriez et al. 1997) and the cloud-top pressure provided by the MODIS instrument (Menzel et al. 2008) to detect multilayered situations. Indeed, they make the hypothesis that clouds for which top pressure is lower than 500 hPa and thermodynamic phase is liquid tend to be multilayered. More recently, Watts et al. (2011) and Sourdeval et al. (2015) showed the feasibility of not only the detection but also the retrieval of two-layer cloud properties using an optimal estimation approach applied to geostationary observations.

The work presented here describes the definition of a cloud multilayer flag based only on measurements from the POLDER sensor, which flew aboard the *Polarization and Anisotropy of Reflectances for Atmospheric Sciences Coupled with Observations from a Lidar* (*PARASOL*) platform from 2006 to 2013. The interests of such a product from a passive remote sensing instrument are multiple. Primarily, the large swath of POLDER observations offers a large spatial coverage. However, POLDER cloud products have been retrieved under the hypothesis of a monolayer cloud, which can induce an important bias. Consequently, a flag indicating the presence of a multilayer cloud structure could improve the quality of the retrievals. Also, such a flag would help in the description of the tridimensional structure of a cloud system. The synergy between information coming from the multidirectional, polarized, and multispectral POLDER measurements is exploited. Our approach is based on a decision tree, which classifies the mono–multilayered cloud scenes. The decision tree implements tests on attributes that were selected based on their information about the mono–multilayer character of a scene. This has been made possible thanks to the coincident observations of POLDER-3/*PARASOL* with those from *CloudSat* and *Cloud–Aerosol Lidar and Infrared Pathfinder Satellite Observations* (*CALIPSO*).

The paper is organized as follows. First, we describe the principle of the detection algorithm: the attributes

that were chosen to distinguish between monolayer and multilayer characters of cloud scenes and then the technique of classification with a decision tree and a metric based on information theory. Second, we provide an evaluation of the decision tree, a physical interpretation of it, and its consistency with an independent approach that uses the receiver operating characteristic (ROC) curve. Then we evaluate statistically the POLDER multilayer flag: we define the notion of classification risk and give arguments toward both a binary mono–multilayer classification and a flag, taking discrete values interpreted as a confidence parameter. During this evaluation, the POLDER multilayer flag is compared with the MODIS one. Finally, we discuss some statistics and the climatology that we obtained about the mono–multilayer character of observed cloud covers.

2. Principle of the detection algorithm

Passive satellite measurements do not intrinsically provide information about the vertical distribution of cloud covers. They are instead more sensitive to column-integrated cloud properties. However, the various interactions between cloudy atmosphere and the radiation field may provide information about different vertical levels in the atmosphere. For example, the penetration depth within cloudy atmosphere of the solar backscattered radiation varies with the scene's angular condition and the different natures (visible/near infrared; use total/polarized) of the exploited radiation. This has been shown, for instance, while estimating cloud effective radius with different types of measurements (Platnick 2000; Bréon and Doutriaux-Boucher 2005). The exploitation of the multidirectional character of measurements in gas absorbing bands also provides information about the cloud vertical profile (Ferlay et al. 2010; Desmons et al. 2013).

a. *A-Train dataset used*

Our approach to discriminate between monolayer and multilayer clouds using POLDER measurements is specifically based on multiple criteria. For doing so, we analyzed a database containing POLDER level-2 data for pixels under the track of the Cloud–Aerosol Lidar with Orthogonal Polarization (CALIOP) and the radar of *CloudSat* with a 5-km horizontal sampling (see details about the CALXTRACT project and CALTRACK files at http://www.icare.univ-lille1.fr/projects/calxtract/). For these coincident pixels, we considered that the lidar and radar echoes provide the "true" cloud vertical locations. The sensitivities of the CALIOP aboard *CALIPSO* (Winker et al. 2007, 2010) and the Cloud Profiling Radar (CPR) aboard *CloudSat* (Stephens et al. 2002, 2008) are suitable for the detection of respectively thin and thick cloud layers, and the combination of their products allows a complete knowledge of the vertical structure of cloud layers. In this work, we have used the *CloudSat* 2B-GEOPROF-lidar product, which provides cloud-base and cloud-top altitudes (LAYERBASE and LAYERTOP) of up to five cloud layers in each atmospheric column. This product identifies a cloudy situation as multilayered only when two layers are vertically spaced at least 960 m apart (Mace et al. 2009). The conversion from altitude to pressure is performed thanks to a local conversion index. Pressures in the atmospheric column come from meteorological reanalyses (Bloom et al. 2005) produced by the NASA Global Modeling and Assimilation Office (GMAO) and are available in *CALIPSO* CAL LID L2-05kmCPro products. Table 1 describes the initial products that served to generate the CALTRACK files we have used for this study. MODIS data are used for the validation of our results.

b. *Information about the multilayer character of cloud structures in POLDER measurements*

First, we studied the distributions of different quantities and differences for monolayer and multilayer cloud scenes. The monolayer/multilayer character is given by the product 2B-GEOPROF-lidar, the scene being declared multilayered when the number of cloud layers found is strictly higher than one. Cloud distributions come from one year of measurements (2008), corresponding to more than 6 600 000 cases. According to the measurements of the lidar CALIOP and the radar CPR aboard the satellite platform and *CloudSat*, 35% of cloudy columns are multilayered over the entire globe at around 1330 LT. The partition between monolayered and multilayered clouds varies with latitude (see in Fig. 1a): over ocean, the proportion of multilayered clouds goes down to 25% outside of the tropics (defined as the area of latitude from −20° to +20°), and within the tropics, up to 50% of the cloud cases are multilayered; over land, the meridian variation of the multilayer proportion is slightly higher, with more multilayer cases in the tropics. Cloudy cases that are selected—population labelled herein as CC095—are close to fully cloudy (POLDER fractional cloud cover > 0.95), and the optical thickness is > 5. The purpose of this selection was to minimize 3D radiative effects and surface effects in POLDER measurements and products. This cloud population represents around 56% of the monolayer cases and 59% of the multilayer cases. The proportion of multilayer cases for this population CC095 is higher than the proportion of it for all cloudy cases: on average, 2.3% more multilayer clouds, the difference being the highest at the tropics, as illustrated in Fig. 1b.

TABLE 1. Level-2 products provided by A-Train sensors used in this study. Products are collocated with lidar shots and sampled every 5 km.

Product	Geophysical product	Horizontal resolution	Sensor (platform)
RB2	Oxygen pressure P_{O_2} Angular standard deviation of P_{O_2}, $\sigma_{P_{O_2}}$ Cloud cover CC Cloud thermodynamic phase Cloud optical thickness τ Geotype index	$18 \times 21\ km^2$	POLDER-3 (*PARASOL*)
2B-GEOPROF-lidar	Number of cloud layers n Cloud-layer top altitudes LAYERTOP Cloud-layer base altitudes LAYERBASE	$2.5 \times 1.4\ km^2$	CPR/CALIOP (*CloudSat*/*CALIPSO*)
MYD06 (collections 5 and 6)	Cloud multilayer flag MLF_{mod} Quality assurance flag QA	$1 \times 1\ km^2$	MODIS (*Aqua*)

Statistical distributions of the following POLDER cloud level-2 products are analyzed: the cloud thermodynamic phase, Rayleigh pressure $P_{Rayleigh}$, oxygen pressure P_{O_2} and its angular standard deviation $\sigma_{P_{O_2}}$, and cloud-top oxygen pressure (CTOP). Both cloud thermodynamic phase and Rayleigh pressure exploit the measurements of the polarization of the upward radiation field, particularly at 443 nm (Buriez et al. 1997). Determination of the thermodynamic phase uses the signature of multi-viewing polarimetric measurements, and the fact that polarimetric radiances saturate for optical thicknesses greater than 2. As a consequence, in the case of multilayer cloud structures, the thermodynamic phase would be of the upper layer if its optical thickness is greater than 2 (i.e., upper-layer optical depth is small relative to the one of the lower layer); otherwise, the signature would be a mixture between liquid and ice clouds and then the thermodynamic phase would be flagged as mixed (Goloub et al. 2000). The oxygen pressure and its angular standard deviation are obtained from the two POLDER measurements in the oxygen A band at 763 and 765 nm (Vanbauce et al. 1998). The oxygen pressure is calculated for up to 16 viewing angles, and the algorithm is based upon the fact that O_2 absorption is linked to the penetration depth of radiation within the atmosphere. The oxygen transmittance T_{O_2} from the top of the atmosphere to a level pressure P and then back to space is estimated by the ratio of POLDER radiances measured in the oxygen A band. As clouds are not perfect reflectors, the photons penetrate the cloud layer, and the photon path depends on the viewing directions and the cloud optical thickness. Then the average oxygen pressure and the angular standard deviation are computed (final products). The cloud-top oxygen pressure is an estimate of the cloud-top pressure and is derived from the oxygen pressure and its standard deviation (Desmons et al. 2013). CTOP has been established for monolayer clouds only, but it is calculated here for all cloudy pixels with the idea that its value for multilayered situations could be singular.

Figure 2 presents the different distributions that result from the year 2008 for monolayered and multilayered cloudy scenes. An ideal distinction of the two populations would correspond to fully separated distributions in a multidimensional domain. Instead, we obtain overlapped distributions with, however, different probabilities in the case of monolayer or multilayer cloudy atmospheres for these quantities to be higher or lower than particular thresholds. Figure 2a shows that for monolayer clouds, the Rayleigh pressure distribution is bimodal, with a maximum at 280 hPa and a second one at 800 hPa. These two modes indicate the presence of high-level and low-level clouds among the cloud population. Concerning multilayer clouds, the distribution is close to a Gaussian centered at 500 hPa and spread out. Figure 2b shows that the distribution of oxygen pressure does not differ significantly between monolayer and multilayer clouds. For CTOP (Fig. 2c), the difference is, on the contrary, more pronounced and resembles that of $P_{Rayleigh}$. This is because CTOP is close to the cloud-top pressure, while P_{O_2} is close to the middle-of-the-cloud pressure. Values above 800 hPa are much more frequent for monolayer clouds and could help to distinguish between the two populations. Figure 2d shows that values taken by the angular standard deviation of oxygen pressure differ a lot for the two populations of cloudy atmospheres: much smaller values are taken for monolayer clouds (smaller than around 20 hPa), while larger values are much more frequent for multilayer clouds. In the case of a single cloud layer, $\sigma_{P_{O_2}}$ is in fact linked to the cloud geometrical thickness (Ferlay et al. 2010; Desmons et al. 2013), while, in the case of multilayer clouds, it is strongly impacted by the vertical distance between the cloud layers. Hence, $\sigma_{P_{O_2}}$ is an interesting discrimination quantity. The metric defined later will show that it is the

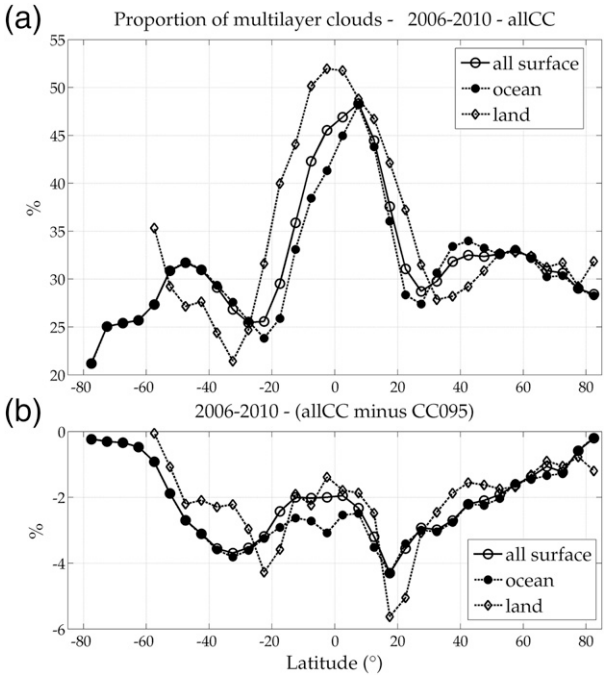

FIG. 1. (a) Proportion of multilayered clouds for all clouds and (b) difference in the proportion between the all-cloud-cover population and the cloud population with POLDER $\tau \geq 5$ and POLDER CC ≥ 0.95 for the period 2006–10 during daytime. The information on the mono/multilayer character comes from *CloudSat–CALIPSO*.

most discriminating criterion. Differences in pressures can also be interesting quantities to consider. Figures 2e and 2f show that such differences often become larger when cloudy atmospheres are multilayered. Indeed, one pressure is close to the lowest pressures of cloud systems, while the other one is close to pressures in its middle (Vanbauce et al. 2003), and a cloud multilayer situation tends to be vertically more extended than a single layer one.

c. *Classification with a decision tree*

We showed above that POLDER parameters can take different values according to the monolayer/multilayer character of cloudy atmospheres. In addition, information about the latitude of the scene and inference of the thermodynamic phase of clouds can help to gain reliability for the estimation of this character (Yao et al. 2010). To propose an objective classification of it, we built a decision tree whose design is based on a chosen metric. This metric quantifies the information about the level of discrimination of each criterion, which leads to a particular design of a decision tree. It is based on actual vertical profiles of cloudy atmospheres and a distinction of their monolayer–multilayer character given by *CloudSat* and *CALIPSO*.

The technique of the decision tree is based on the idea of classifying an object through a set of tests on the attributes that describe it. These tests are organized in a way that the answer to one of them indicates the next test to be performed. The tests are organized as a tree, from a root to leaves (top-down induction). A leaf of the tree indicates one of the classes, and a test concerning one or more attributes is associated with each node. In our situation, the objects are the monolayer–multilayer situations, and the attributes are the quantities sensitive to this character. The metric used to make the choice of the right attributes comes from information theory.

1) INFORMATION THEORY

A probabilistic interpretation of decision tree designing is given by Cornuéjols and Miclet (2010) and is based on information theory, developed by Claude Shannon in the 1940s. Shannon and Weaver (1949) make the link between information and the entropy of probability density. Entropy is here very close to the thermodynamic formulation given by Gibbs, where it represents the logarithm of the number of distinct states contained in a system. The entropy of a variable w that can take the values $\{w_j\}_{j\in\mathcal{C}}$ with probabilities $p(w_j)$ is defined as

$$H(w) = -\sum_{j\in\mathcal{C}} p(w_j)\ln p(w_j). \tag{1}$$

The logarithm is expressed in base 2 to be able to describe the information using a binary base, and entropy is expressed in bits. In this work, w stands for the mono–multilayer character; thus, the number of classes $\mathcal{C}$ is equal to 2. Entropy $H(w)$ defines the uncertainty that we have about the knowledge of w. As attributes are sensitive to the monolayer–multilayer character of a cloudy situation, we consider now attributes a that can take the values $\{a_i\}$ and define entropy conditioned on a, or conditional entropy, as

$$H(w\,|\,a) = -\sum_{i,j} p(w_j \cap a_i)\ln p(w_i\,|\,a_i), \tag{2}$$

where $p(w_j \cap a_i)$ and $p(w_i\,|\,a_i)$ are joint probability distribution and conditional probability, respectively. The quantity $H(w\,|\,a)$ represents the uncertainty on the monolayer–multilayer character knowing the response to the test on a. The more the quantity a allows the differentiation of the values of w, the smaller is the entropy $H(w\,|\,a)$. If $a = w$, the entropy is equal to 0: knowing w removes the uncertainty on w. Finally, we consider the quantity

$$I(w,a) = H(w) - H(w\,|\,a). \tag{3}$$

The quantity $I(w, a)$, called mutual information (Cover and Thomas 1991), quantifies the reduction in the uncertainty in w due to the knowledge of a. It measures the statistical dependence between w and a. A decision tree that should classify the monolayer–multilayer character w of a cloudy scene will use attributes that reduce the

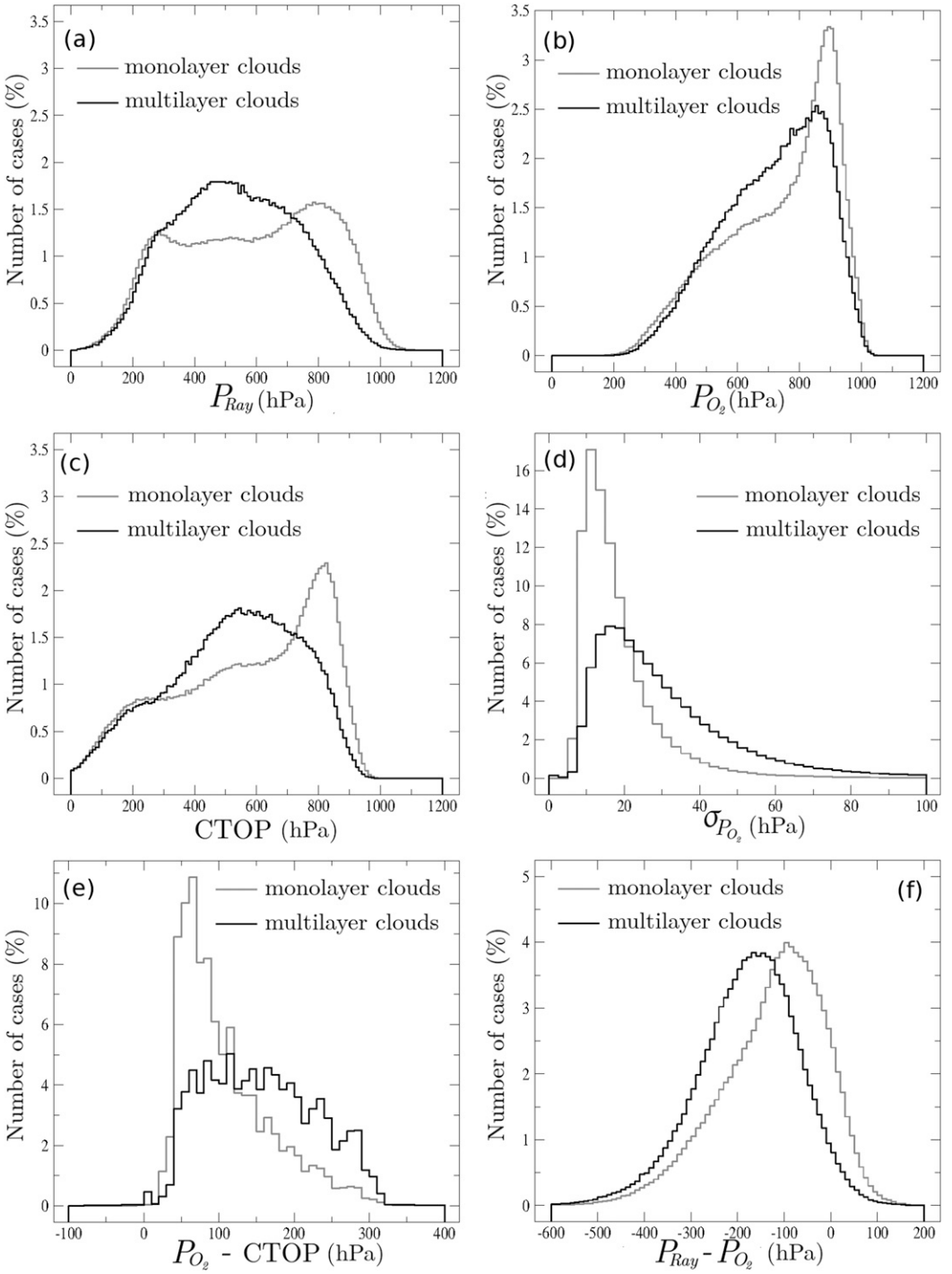

FIG. 2. Histograms of (a) Rayleigh pressure, (b) oxygen pressure, (c) angular standard deviation of the oxygen pressure, and (d) CTOP and of the differences (e) between oxygen and CTOP and (f) between Rayleigh and oxygen pressures. Histograms are plotted for monolayered (gray lines) and multilayered (black lines) clouds, for which $\tau \geq 5$ and CC ≥ 0.95 in 2008. The information on the monolayer or multilayer character comes from the *CloudSat* coproduct 2B-GEOPROF-lidar.

uncertainty about this character. At a certain node of the tree, the choice of the attribute a that is to be considered corresponds to the one that minimizes the uncertainty about w or, equivalently, the one that minimizes the quantity $H(w\,|\,a)$. And the probabilities of branches are conditional on the event associated with the parent node.

2) DESIGNING THE DECISION TREE

Data from 2008 form a learning set of 2 798 792 cloudy pixels detected by POLDER, CALIOP, CPR, and MODIS, above land and ocean, for which the cloud cover is ≥0.95 and the cloud optical thickness is ≥5 (both are provided by POLDER measurements). Among those, according to CALIOP and CPR, 1 802 422 pixels contained monolayer clouds, and 996 370 were multilayered cloudy columns. The proportion of monolayer (multilayer) clouds is thus 65% (35%). Each cloudy case is described by different attributes: the cloud thermodynamic phase; whether the pixel is or is not in the tropical area; and the P_{Rayleigh}, P_{O_2}, $\sigma_{P_{O_2}}$, CTOP, $P_{\text{Rayleigh}} - P_{O_2}$, and $P_{O_2} -$ CTOP pressure parameters. Except for the thermodynamic phase, which can take three values (liquid, ice, or mixed), all the attributes give binary information from a binary rule: a pixel is located or not in a tropical area; pressure parameters are higher or lower than a threshold value.

Ideally, one would try to design a classification tree with final leaves as pure as possible, through successive nodes and their associated binary tests attributes. It would mean that attributes bring enough information to make perfectly the distinction between monolayer and multilayer situations. It is not the case here. Instead, nodes are successively designed up to a step where entropy cannot be reduced further. Then, the proportion of monolayer and multilayer clouds is computed for each leaf of the tree and is retained as a multilayer indicator.

Initially, without considering attributes that bring information, the entropy of the variable "character monolayer or multilayer," denoted as mo − mu and H(mo − mu), is equal to 0.943. To reduce the uncertainty in the variable mo − mu, we calculate the entropy conditioned on the different attributes that we considered. For the attribute concerning the latitudinal location of the pixel and the phase of the cloud, the test is binary (inside/outside the tropical zone, liquid or not, mixed or not, and ice or not). For pressure parameters, the test is the following: Is the attribute smaller than a given threshold? The entropy of the variable mo − mu conditioned on pressure parameters is thus computed for different thresholds, ranging between two values determined for each parameter. The threshold that will be retained is the one that minimizes the entropy. For example, for the oxygen pressure, the entropy $H(\text{mo} - \text{mu}\,|\,P_{O_2})$ varies between 0.924 and 0.946, as shown in Fig. 3, the minimum being reached when the threshold is equal to 850 hPa. Calculations of conditional entropy for the different attributes are summarized in the top half of Table 2.

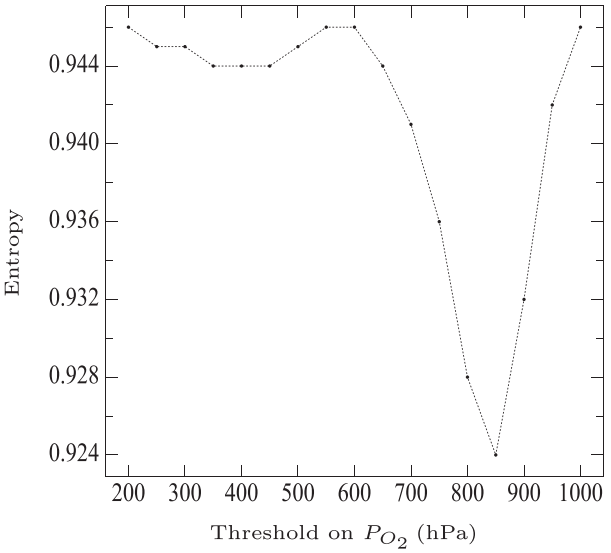

FIG. 3. Entropy of the character monolayer/multilayer conditioned by a threshold on the oxygen pressure P_{O_2}. The threshold varies between 200 and 1000 hPa in increments of 50 hPa.

The attribute that minimizes the entropy of the variable mo − mu is the angular standard deviation of the oxygen pressure $\sigma_{P_{O_2}}$, for a threshold equal to 22.5 hPa. Thus, the test on $\sigma_{P_{O_2}}$ will constitute the first node (i.e., at the root) of the decision tree. This is consistent with the observation made in Fig. 2d, which shows two very distinct distributions of this attribute. Then, the decision tree is further designed by separating the pixels into two groups: the ones that respect the criterion "$\sigma_{P_{O_2}} \leq$ 22.5 hPa" and the others. In the first branch, 75% of cloudy cases are monolayered. Again, we calculate the entropy of the quantity mo − mu conditioned on attributes for selected pixels (for this branch, the selection rule is $\sigma_{P_{O_2}} \leq$ 22.5 hPa). The new minimum of the entropy of mo − mu is obtained from the attribute P_{Rayleigh} with a threshold equal to 750 hPa (details of the calculation are given in the bottom half of Table 2). We go on designing the different branches and nodes of the tree following the same rule. The designing of the tree is stopped at the fourth level of nodes that become leaves. As we have used data from 2008 to build the tree, we used data from 2007 for validation. The tree remains stable, and it is the one obtained for 2007, which is represented in Fig. 4.

3. Analysis and validation of the approach

The decision tree was obtained by applying a general method based on information theory. It quantifies and

TABLE 2. Entropies conditioned on the different attributes.

Attribute	Entropy	Threshold value (hPa)
	All clouds	
—	$H(\text{mo} - \text{mu}) = 0.943$	—
Lat	$H(\text{mo} - \text{mu} \mid \text{lat}) = 0.939$	—
Phase	$H(\text{mo} - \text{mu} \mid \text{phase}) = 0.938$	—
P_{O_2}	$0.924 \leq H(\text{mo} - \text{mu} \mid P_{O_2}) \leq 0.946$	850
$\sigma_{P_{O_2}}$	$0.895 \leq H(\text{mo} - \text{mu} \mid \sigma_{P_{O_2}}) \leq 0.944$	22.5
P_{Rayleigh}	$0.896 \leq H(\text{mo} - \text{mu} \mid P_{\text{Rayleigh}}) \leq 0.945$	750
CTOP	$0.899 \leq H(\text{mo} - \text{mu} \mid \text{CTOP}) \leq 0.945$	750
$P_{\text{Rayleigh}} - P_{O_2}$	$0.908 \leq H(\text{mo} - \text{mu} \mid \delta_{P_{\text{Rayleigh}} - P_{O_2}}) \leq 0.946$	−100
$P_{O_2} - \text{CTOP}$	$0.913 \leq H(\text{mo} - \text{mu} \mid \delta_{P_{O_2} - \text{CTOP}}) \leq 0.946$	100
	Clouds for which $\sigma_{P_{O_2}} \leq 22.5$ hPa	
—	$H(\text{mo} - \text{mu})_{\sigma \leq 22.5} = 0, 811$	—
Lat	$H(\text{mo} - \text{mu} \mid \text{lat})_{\sigma \leq 22.5} = 0, 807$	—
Phase	$H(\text{mo} - \text{mu} \mid \text{phase})_{\sigma \leq 22.5} = 0, 810$	—
P_{O_2}	$0.794 \leq H(\text{mo} - \text{mu} \mid P_{O_2})_{\sigma \leq 22.5} \leq 0, 810$	800
P_{Rayleigh}	$0.772 \leq H(\text{mo} - \text{mu} \mid P_{\text{Rayleigh}})_{\sigma \leq 22.5} \leq 0, 810$	750
CTOP	$0.787 \leq H(\text{mo} - \text{mu} \mid \text{CTOP})_{\sigma \leq 22.5} \leq 0, 810$	750
$P_{\text{Rayleigh}} - P_{O_2}$	$0.779 \leq H(\text{mo} - \text{mu} \mid \delta_{P_{\text{Rayleigh}} - P_{O_2}})_{\sigma \leq 22.5} \leq 0, 810$	−100
$P_{O_2} - \text{CTOP}$	$0.799 \leq H(\text{mo} - \text{mu} \mid \delta_{P_{O_2} - \text{CTOP}})_{\sigma \leq 22.5} \leq 0, 810$	100

compares the information about the mono–multilayer character of cloud cover coming from the values taken by different attributes. We give below a first evaluation of the decision tree by comparing its classification with results given by an independent approach based on the ROC plot. Then we discuss the physical meaning and consistency of the main cloud classes obtained from the tree.

a. *Evaluation with ROC curve: decision at the root of the tree*

The ROC makes it possible to evaluate the performance of a binary classification rule. Since the 1950s, this tool has found extensive usage in psychophysics (Green and Swets 1966) and machine learning (Fawcett and Provost 1996; Hand and Till 2001) to evaluate medical diagnostic tests (Hanley and McNeil 1982; Swets 1988) and also in atmospheric sciences (Olson 1965; Wilks 1995; Mason and Graham 1999; Gabriel et al. 2009). This method not only considers the error rate of a binary classification but also the number of false positives and of false negatives. The interest of it is that the cost of misclassification can be asymmetric, and sometimes, one prefers to reduce the more expensive kind of errors, even if this leads to a higher error rate (Cornuéjols and Miclet 2010). For example, when the classification deals with a medical diagnostic, physicians prefer to increase the number of false alarms instead of the number of missed disorders: false positive cases are less expensive than false negative ones.

Here, the diagnostic concerns the mono–multilayered character of cloud cover as classified by the decision tree. The choice of the binary distinction at each node of the tree can be evaluated with the ROC plot. Figure 5 shows such plots for the decision at the root of the tree, before the first node. The ROC is a plot of the true positive rate (TPR) versus false positive rate (FPR). They correspond in our study to the fraction of monolayered cases correctly identified by POLDER following a classification rule and the fraction of multilayered cases misclassified by it as monolayered. Each curve corresponds to a discriminating attribute, and any point on the curves is determined by a particular threshold of the attribute, the variety of it being the same as the ones used when designing the decision tree. For the latitude and thermodynamic phase parameters, curves are reduced to only one point that corresponds to a unique binary distinction (inside/outside tropics, liquid or not, etc.). A perfect classification criterion would provide a point of coordinates (0, 1), which would signify a sensitivity equal to 100% (no false negative) and an FPR equal to 0. A random classification would produce a point along the diagonal that links the bottom left and top right corners (called the line of no discrimination). Points situated above this diagonal stand for a useful criterion (better than hazard), while points below it represent a bad criterion. Considering equally the two costs of misclassification (monolayered or multilayered), the best criterion is the one for which the distance between a point on the curve and the coordinate (0, 1) is the shortest.

Figure 5 shows that, apart from phase criterion and the parameter CTOP − P_{Rayleigh}, which are very weakly discriminative, the chosen parameters can bring a significant discrimination: points can be way above the

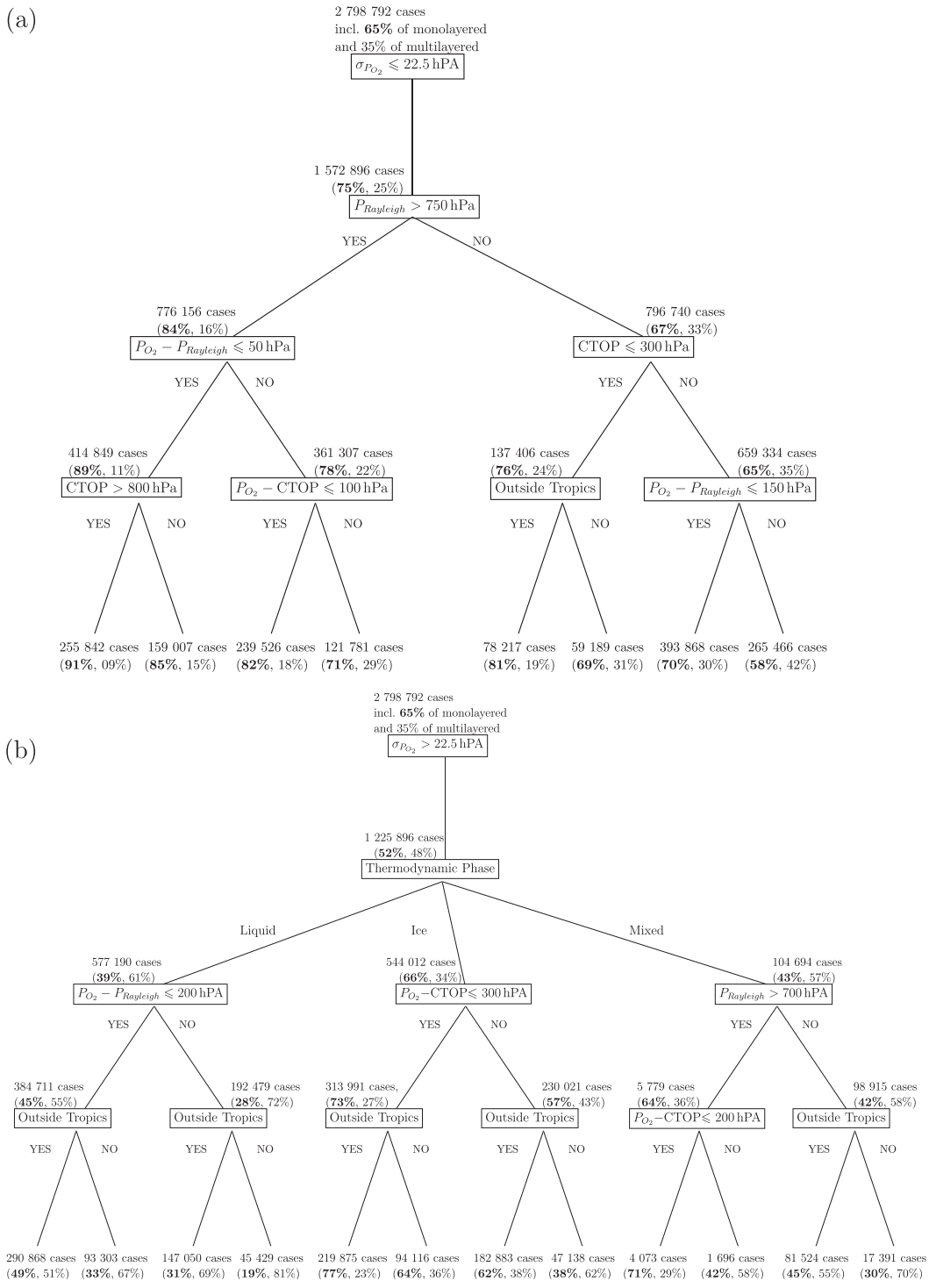

FIG. 4. (a) "Left" limb ($\sigma_{P_{O_2}} \leqslant 22.5\,\text{hPa}$), and (b) "right" limb ($\sigma_{P_{O_2}} > 22.5\,\text{hPa}$) of the decision tree for the distinction of monolayered and multilayered cloud structures. For every test at every node, the number of concerned clouds as well as the proportion of monolayered (boldface type) and multilayered structures are given. The tree has obtained its learning from the CALIOP/CPR track using data from 2008 and then applied to 2007. The values given are those from 2007.

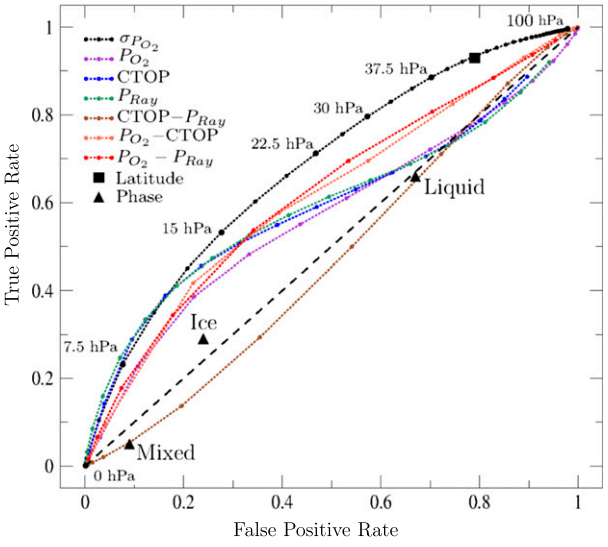

FIG. 5. ROC at the root of the decision tree. TPRs and FPRs are given following the classification of all cloudy scenes as monolayered or multilayered from tests on the different attributes with different thresholds. Data are from 2009. Values of threshold on the angular standard deviation $\sigma_{P_{O_2}}$ are emphasized. Curves are shrunk to a unique point when the criteria of classification are based on a unique threshold.

diagonal for some thresholds, as for P_{Rayleigh}, CTOP, and $P_{O_2} - P_{\text{Rayleigh}}$. The angular standard deviation of the oxygen pressure $\sigma_{P_{O_2}}$ appears as a highly discriminating parameter, and the best classification corresponds to a threshold on $\sigma_{P_{O_2}}$ of around 20 hPa. This corroborates the calculations of entropy made in the previous paragraph and confirms the choice of $\sigma_{P_{O_2}}$ as the first node of the tree with a threshold value of 22.5 hPa.

b. *Physical analysis of the tree*

Although the attributes chosen for the distinction of monolayered and multilayered situations have been chosen from a physical understanding of these situations, the decision tree has been obtained by applying a rigorous but general method based on objective and quantitative criteria. In the following paragraph, we propose to detail the physical rationale behind these criteria and to analyze the portrait of the main populations obtained by this classifier.

Leaves from the left branch of the tree (Fig. 4a) concern clouds for which the angular standard deviation of the oxygen pressure is lower or equal to 22.5 hPa. This means that the variability of the photon pathlength inside the cloudy layer according to the different viewing directions is quite limited. Clouds belonging to leaf 1 with a monolayer confidence index of 91% (≈10% of the cloudy situations) present a Rayleigh pressure higher than 750 hPa and a pressure CTOP higher than 800 hPa, which corresponds to low clouds with a top altitude smaller than 2.5 km. Leaf 7 shows a monolayer confidence index of 70% (≈14% of the cloudy situations) and describes middle to high clouds ($P_{\text{Rayleigh}} \leq 750$ hPa and CTOP > 300 hPa) that also have a limited vertical extent ($P_{O_2} - P_{\text{Rayleigh}} \leq 150$ hPa). They are indeed probably cirrus or altostratus, monolayer cloud types.

The right branch of the tree concerns clouds for which the angular standard deviation of the oxygen pressure is higher than 22.5 hPa (Fig. 4b). This important angular variability of the directional oxygen pressure indicates clouds that tend to get away from the model of the perfect reflector. As would be expected, the second node on this branch concerns the thermodynamic phase, as the relationship between angular standard deviation of oxygen pressure and cloud geometrical thickness is highly influenced by the scattering phase function and hence the thermodynamic phase (Ferlay et al. 2010). The nodes that lead to leaf 4, with the multilayer confidence index of 81%, concern liquid water clouds located in tropical areas and for which $P_{O_2} - P_{\text{Rayleigh}} > 200$ hPa. These criteria are consistent with characteristics of multilayer clouds. Likewise, leaf 12, which displays a multilayer confidence index of 70%, concerns clouds with a thermodynamic phase identified as mixed, which indicates a rather complex microphysics or potentially multilayer situations (Riédi et al. 2010). These clouds are found at middle to high altitudes ($P_{\text{Rayleigh}} \leq 700$ hPa), and are located in the tropical region. These characteristics are compatible with multilayered situations often met in this region.

4. Definition of a multilayer flag and first evaluation

A first validation of the design of the decision tree comes from the stability of the results obtained for different years and the consistency of the result coming from the tree's metric with the one from the ROC approach. Each POLDER elementary pixel falls into the tree down to 1 of the 20 leaves that were defined. To evaluate our classification rule, we need to define a multilayer indicator, or flag, from the tree's classification to be able to compare it with other approaches. This is what we perform here, followed by a first qualitative comparison between POLDER multilayer classification and the one from MODIS for one case study.

a. *Definition of a multilayer flag*

The scores in percent obtained at each final leaf of the decision tree represent a statistical confidence in the monolayer–multilayer character of particular cloudy scenes that were equally classified throughout the tests of the tree. We chose to define a multilayer flag MLF_{pol} defined as

$$\mathrm{MLF_{pol}} = 100 - (\text{leaf's monolayer probability score in percent}). \quad (4)$$

Thus, $\mathrm{MLF_{pol}}$ takes discrete values between 0 and 100. Values closest to 0 indicate a higher confidence in the monolayer character and closest to 100, a higher confidence in the multilayer character. This indicator can be used as it is, a confidence in the vertical partition of atmospheric hydrometeors in one or more than one layer. It may also lead to a binary classification between monolayer and multilayer clouds.

It is interesting and challenging to compare this multilayer classification with another one coming from a different approach or measurement. An opportunity is offered at the pixel level and over a long-time period thanks to the coincidence of numerous *PARASOL* and MODIS/*Aqua* measurements under the *CALIPSO*/*CloudSat* track, all platforms being part of the A-Train.

The value of the MODIS multilayer flag ($\mathrm{MLF_{mod}}$) is the result of the success of independent multilayer tests. When more tests are positive, the value of the scientific dataset (SDS) Cloud_Multi_Layer_Flag increases from 2 to 8 for MODIS collection 5 (Wind et al. 2010) and from 2 to 9 for collection 6 (Platnick et al. 2015). The value 1 for $\mathrm{MLF_{mod}}$ indicates single-layer clouds. In collection 6, the multilayer detection has been updated, and a Pavolonis–Heidinger (PH) test (Pavolonis and Heidinger 2004) is added. Information about each test result is kept in the sixth byte of the Quality_Assurance_1km SDS. We followed the recommendation of Platnick et al. (2015) and interpret cases where only the PH multilayer test is positive as single cloud cases. They represent around 9% of all the cloudy cases over the temporal period of study. The value 0 means not only clear-sky cases but also cases where there was no cloud optical property retrieval. They represent around 13% of all cloud cases.

The MODIS parameter $\mathrm{MLF_{mod}}$ actually indicates valid but potentially problematic effective radius retrievals, caused mostly by multilayer situations. While based on totally different approaches and metrics, $\mathrm{MLF_{pol}}$ and $\mathrm{MLF_{mod}}$ can be qualitatively compared as low values of the flags indicate single-layer scenes and high-value, multilayer scenes. Another comparison is also possible once a binary distinction is defined for each flag.

b. *Qualitative evaluation on one case study*

Figure 6a shows a red–green–blue (RGB) representation in true colors (I) and in false colors (II) of a cloud scene as it was observed by MODIS (bands 1, 4, and 3 and 7, 2, and 1, respectively) on 24 September 2008, southeast of South Africa. Stratocumulus low-level clouds can be seen on the southwestern part of the image with mostly closed cells. In the other part of the domain, the cloudy situation is more complex, with convective cells of different sizes and the large presence of cirruslike ice clouds. The figure in false colors (panel II) reveals slightly more clearly that some high-level clouds seem to lie above liquid ones at lower altitudes, with an optical thickness small enough so that the lowest cloud layer is visible. In the southeastern part of the domain, the perturbation effect of the Kerguelen Islands on the flow of low-level atmospheric layers is even visible, while the surrounding area seems covered by cirrus clouds.

Figure 6b shows the maps of the multilayer flag from MODIS collection 5 (C5) and *PARASOL*. Despite the facts that MODIS and POLDER sensors do not have the same footprint or the same pixel resolution (see Table 1), the figure shows a clear consistency between POLDER and MODIS: they both describe the low-level clouds as single-layer clouds, and they both indicate a high probability of multiple cloud layers in the same areas.

For POLDER and MODIS measurements that are coincident with the shots of the satellite lidar and radar, that is, on the green line in Figs. 6a and 6b, precise information about the vertical location of clouds is available from CALIOP and CPR. Figure 6c shows the values of POLDER and MODIS multilayer flags for those locations as well as the true cloud vertical partition, with black and green flags in the monolayer and multilayer cases, respectively. For the convenience of comparison, MODIS flags are multiplied by a factor of 10. The value 1 for $\mathrm{MLH_{mod}}$, so a 10 here, indicates single layer, and higher values indicate cloud multilayered structures with an increasing confidence. The figure shows how complex and different the vertical partition of cloud scenes can be and the classification by the different instruments and algorithms of each particular cloud scene. For example, the monolayer cases in the southernmost and northernmost parts of the domain (black flags) are classified by *PARASOL* with low values of $\mathrm{MLF_{pol}}$. These values are smaller than the threshold value of 44, a classification that identifies these cases as monolayered with, as we will see below, an overall minimization of the POLDER risk of multilayer misclassification. MODIS C5 and collection 6 (C6) multilayer flags also take low values mostly equal to one, indicating monolayer cloud scenes. At some locations, MODIS C6 takes the value 4 while clouds are monolayered, and the quality assurance (QA flag indicates the only success of the PH test. It confirms the

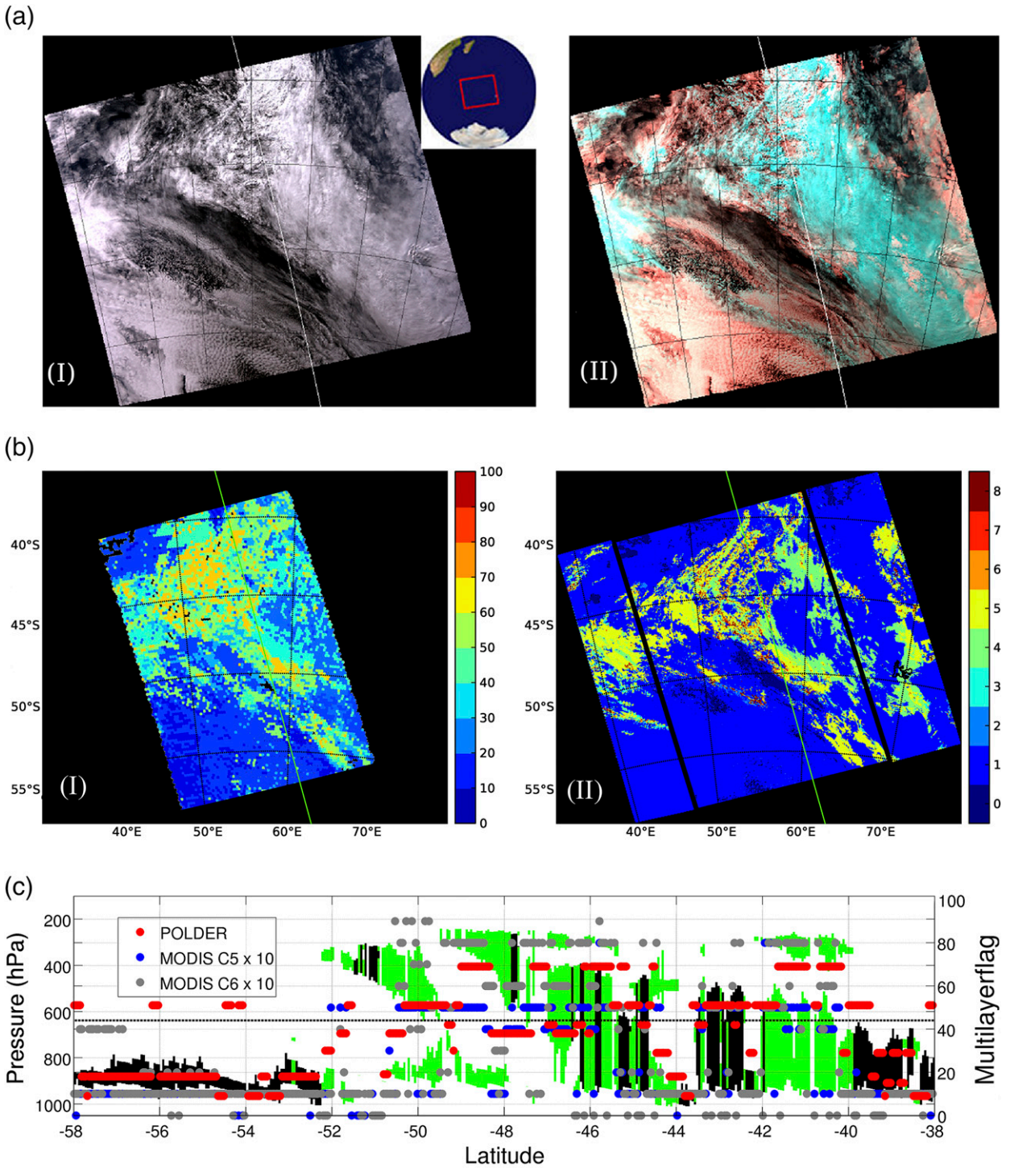

Fig. 6. (a) MODIS RGB imagery, as described in the text. (b) *PARASOL* (I) and MODIS C5 (II) multilayer flags. (c) Values of POLDER (red) and MODIS C5 (blue) and C6 (gray) multilayer flags under the CPR/CALIOP track at a horizontal sampling of 5 km for a cloud scene on 24 Sep 2008. In (a) and (b), the straight green line indicates the track of *CloudSat* and CALIOP. In panel II of (b), the POLDER swath is indicated by a black box to help the comparison. In panel I of (b), low values indicate single-layer clouds and high values indicate multilayer clouds with increasing confidence for POLDER. In panel II of (b), 1 indicates a single-layer cloud, and values from 2 to 8 indicate a multilayer situation with increasing confidence for MODIS C5. In (c), the cloud vertical cross sections from the CPR/CALIOP are flagged in black for monolayer cases and in green for multilayer cases; the horizontal dashed line gives the threshold that minimizes the risk of misclassification between monolayer and multilayer cases with POLDER.

TABLE 3. Confusion matrix for a multilayer indicator.

	Real class		
Estimated class	Monolayered (P)	Multilayered (N)	Sum
Monolayered	TP	FP	EP
Multilayered	FN	TN	EN
Sum	*P*	*N*	*t*

comment of Platnick et al. (2015) stating that the PH algorithm can be overly aggressive in flagging multilayered scenes. Most of the multilayer scenes (two or three cloud-layer scenes with green flags) come with higher values of the three flags (POLDER and MODIS C5 and C6). This is the case between latitudes 42° and 40°S and between 50° and 46°S. At some locations, the multilayer diagnostic is difficult (see around the latitude 44.5°S), which is certainly due to the higher optical depth of the upper cloud layer.

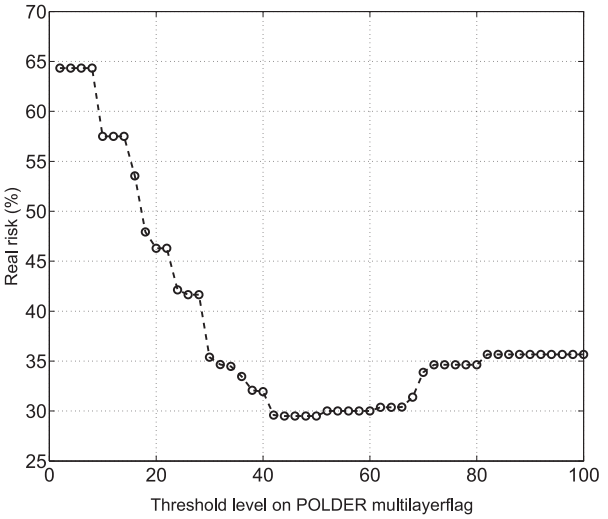

FIG. 7. Real risk associated with POLDER pixel classification for different thresholds on the multilayer flag MLF. All cloudy pixels in 2008 with POLDER cloud cover >0.95 and cloud optical depth >5.

5. Global performance of the POLDER multilayer flag

The POLDER cloud multilayer flag defined above provides precisely a statistical confidence in the mono–multilayer character of each cloud scene. This multilayer flag can be used as it is: smaller (larger) values mean higher confidence in the monolayer (multilayer) character of cloud scenes. This flag can be a guide for a careful use of cloud parameters, which are largely retrieved under the monolayer assumption. For climatological applications, for example, the value of the flag could define which cloudy pixels should be considered or rejected in the statistics. We propose to define from this multilayer flag a binary distinction: a cloud scene is classified as either monolayered or multilayered. A binary distinction offers several advantages. It allows an optimization of the handling of data with a minimization of misused scenes and a quantification of the classification's performance with calculation of its associated risk and confidence. And it permits the comparison of different classifications based on different metrics.

a. *Mono–multilayer binary distinction, risk, and confidence*

Considering the definition of the POLDER multilayer flag, a binary classification rule based on a unique threshold T on the multilayer flag is the following: if $\mathrm{MLF_{pol}} \leq T$, the cloudy scene is described as being monolayered, and if $\mathrm{MLF_{pol}} > T$, as multilayered. For each value of T, we compute the statistical risk of misclassification by POLDER and the confidence in the monolayer (multilayer) character when a pixel is classified as monolayer (multilayer). The definition of the best binary distinction corresponds to the value of T that minimizes the risk of misclassification.

To compute risk and confidence, we built the confusion matrix of the classification rule (see Table 3), which makes it possible to compare the estimated mono–multilayer character with the true one (given by *CloudSat*/*CALIPSO*). The confusion matrix defines true positive (TP), false positive (FP), and estimated positive (EP) pixels, as well as true negatives (TN), false negatives (FN), and estimated negatives (EN), when cloudy pixels are classified as monolayered (positives) or multilayered (negatives). "Estimated" positives (negatives) describes the number of clouds identified as monolayered (multilayered) by our algorithm. If we consider that all errors are equally significant, that is, that the cost of misidentifying a monolayer or a multilayer scene is equal, the sum of the nondiagonal elements of the confusion matrix divided by the size of the dataset t gives an estimate of the real risk of misclassification:

$$\mathrm{real\_risk} = \frac{\mathrm{FP} + \mathrm{FN}}{t}. \tag{5}$$

The confidences in the qualifiers "monolayered" and "multilayered" are obtained with

$$C_{\mathrm{mono}} = \frac{\mathrm{TP}}{\mathrm{EP}} \quad \text{and} \quad C_{\mathrm{multi}} = \frac{\mathrm{TN}}{\mathrm{EN}}. \tag{6}$$

Figure 7 shows the real risk associated with POLDER classification for different values of the threshold level T on $\mathrm{MLF_{pol}}$. The cloud population consists of all cloudy pixels in 2008 with a POLDER cloud cover higher than

TABLE 4. Confusion matrices in percent for the POLDER and MODIS multilayer flags over the period 2006–10.

	Real class (*CloudSat–CALIPSO*)		
Estimated class	Monolayered (P)	Multilayered (N)	Sum
POLDER multilayer confidence index for a threshold of 44%			
Monolayered	53.1	18.7	71.8
Multilayered	11.8	16.4	28.2
Sum	65.0	35.0	100
MODIS collection 5			
Monolayered	51.9	19.1	71.0
Multilayered	12.6	16.4	29.0
Sum	64.5	35.5	100
MODIS collection 6			
Monolayered	51.1	18.9	70.0
Multilayered	13.9	16.1	30.0
Sum	65.0	35.0	100

0.95 and cloud optical depth higher than 5, noted as CC095. The real risk is around 64% when $T = 0$ and 36% when $T = 100$: these are the global probabilities that cloud scenes are monolayered and multilayered. When the threshold is low, the confidence C_{mono} is higher, with very few cloudy pixels classified as monolayered, and the confidence C_{multi} is very low. The reverse is obtained for threshold values close to 100. The two confidences range respectively from 92% down to 65% for C_{mono} and from 35% up to 78% for C_{multi} when the threshold goes from 0 to 100. For a particular value of the threshold level, $T = 44$, the real risk is minimum and equals 29.5%. The existence of a minimum on the curve validates this approach for a binary distinction and its interest: while the decision tree helps to discriminate cloudy pixels according to their mono–multilayer feature, there is also a best way, all errors of classification being equally significant, to make an objective binary distinction between pixels. For this chosen threshold level of 44, we did compute the confusion matrix for the cloud population CC095 over the period 2006–10 and for all surface types (top matrix in Table 4). It shows first that POLDER tends to overestimate the global proportion of monolayer clouds (71% against 65%). This result is consistent with the fact that POLDER hardly distinguishes very thin cirrus above a lower cloud deck. Around 82% of monolayered clouds and 47% of multilayered are well classified. Confidences are $C_{\text{mono}} = 74.0\%$ and $C_{\text{multi}} = 58.2\%$, and the real risk over that period is 30.5%. These numbers result from the fact that POLDER identifies a significant fraction of cloud multilayer scenes as monolayer and some monolayer scenes as multilayer.

For comparison, we defined a binary multilayer classification for MODIS and computed the corresponding confusion matrix: a value equal to unity for MLF_{mod} indicates a monolayer cloud case, while a value larger indicates a multilayer one. Concerning the MODIS C6 multilayer flag, we followed the recommendation of Platnick et al. (2015) and considered carefully the quality assurance byte 6 setting. The confusion matrices in the middle and bottom of Table 4 show that MODIS C5 and C6 flag performances are very close to the one of POLDER. The real risks with MODIS C5 and C6 are 31.7% and 32.8%; their confidences C_{mono} and C_{multi} are 73.1% and 56.6% (73.0% and 53.7%, respectively). It should be noted that not accounting for the QA information would lead to a quite different MODIS C6 result and performance, with only 55% of monolayered cases identified (against 70%), a lower value of C_{multi}, and a global higher real risk. It confirms again the previous analysis about the importance of MODIS QA information.

To analyze and compare with more details the statistical performance of the multilayer flags, we computed monthly mean risk and confidences with a 3-month window and over the entire globe (Fig. 8) and the zonal variation of these quantities over the 5 yr (Figs. 9a–c). Beside the cloud population CC095 that served as a learning database, we considered also the whole cloud population without restriction (noted as allCC). Considering first the cloud population CC095, Fig. 8 shows that the POLDER risk of misclassification is quite constant over the period, with a similar limited seasonal variation over the years. Figure 9a shows, however, that the POLDER zonal risk varies, with a maximum in the tropics. This enhanced risk in the tropics—where there is a maximum proportion of multilayer scenes (see Fig. 1a)—is associated with a decrease in the confidence in the monolayer character C_{mono} (Fig. 9b), while the confidence in the multilayer character C_{multi} is high there (Fig. 9c). Figure 8 shows also the agreement of POLDER and MODIS (particularly C5) monthly mean results for the cloud population CC095, MODIS risks of misclassification being slightly higher. MODIS risks are actually smaller than POLDER ones out of the tropics but significantly higher within the tropics (see Fig. 9a). These higher risks are again associated with a decrease of C_{mono}. Results show also that the performance of the POLDER classification is much weaker when the cloud cover is less homogeneous and optically thick. The degradation concerns all months and all latitudes and comes from a significant decrease in the confidence C_{multi}. Some cloud monolayer scenes with $\text{CC} < 0.95$ and low cloud optical depth are actually interpreted as being multilayered by the POLDER indicator. The monolayer character is less affected by CC: multilayered scenes with $\text{CC} < 0.95$ are not interpreted as being monolayered. It is not a surprise that the horizontal

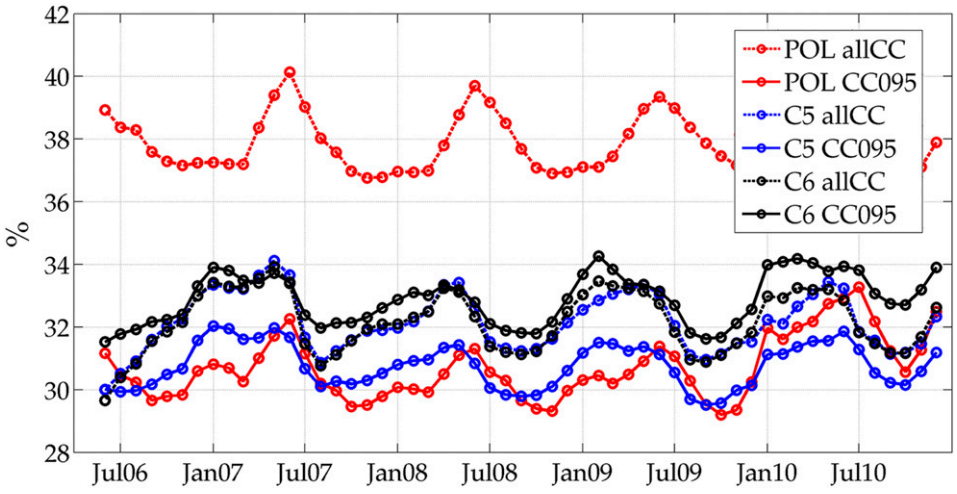

FIG. 8. Monthly mean real risk of the multilayer classification with a 3-month window from POLDER (POL) and MODIS C5 and C6 and for all surfaces.

heterogeneity of a cloud scene is also an issue for the correct remote estimation of its cloud vertical partitioning. It is particularly the case for POLDER, certainly, because the decision tree described above was trained with a population of clouds with CC ≥ 0.95 and $\tau > 5$. The risk obtained for land surfaces only—not shown here—is between 4% and 7% higher when compared with cases over ocean, and MODIS results show also a sensitivity to the difference in the two cloud populations allCC and CC095.

b. *Inferred mono/multilayer climatology*

Having considered a binary distinction between monolayer and multilayer cloud scenes from the passive instruments POLDER and MODIS, a global climatology of this binary cloud distinction can be obtained and compared with the reference shown in Fig. 1a. It is another way to challenge the capacity of the multilayer flags. Here, only observations of the passive sensors obtained under the CALIOP/*CloudSat* track were used. Figure 10a shows the zonal proportion of monolayer clouds inferred from *PARASOL* and MODIS over the ocean and the period 2006–10 and for cloud scenes with a cloud cover CC ≥ 0.95 and $\tau \geq 5$. The true proportion from the lidar and the radar is indicated with the thick green curve. The figure shows that POLDER is able to provide correctly the global feature of this climatology, with a minimum fraction of monolayer cases in the tropics, a rapid increase of it between latitudes 20° and 30°, and a quite constant fraction up to 70° of latitude. However, POLDER tends to overestimate the occurrence of monolayer cases and particularly at midlatitudes. It is certainly a limit of the POLDER retrieval due to optically thin cirrus clouds overlying a lower cloud deck, cirrus that POLDER does not discern. MODIS C5 and C6 (blue and black lines) provide a more reasonable proportion of monolayered clouds at midlatitudes as compared with POLDER. It is certainly due to a higher sensitivity of MODIS parameters, and among them the multilayer classification, to thin cirrus clouds, as illustrated in Wind et al. (2010) in their Fig. 7. However, the global climatologies provided by MODIS C5 or C6 are quite different: the inferred fractions of monolayer clouds increase in the tropics relative to midlatitudes, which is the inverse of the climatology obtained from CALIOP/*CloudSat*. It should be remembered again that the MODIS multilayer classification indicates issues on effective radius retrieval and inconsistency in cloud phase retrieval that might be due to multilayer situations. Two layers of ice clouds, for example, might cause no inconsistency in the retrieval and be classified as a single cloud case. Actually, the proportion of monolayer cases when only the C6 PH test is positive is around 50% in the tropics and more than 75% out of it. Considering those cases as monolayered situations instead of multilayered leads to a rather good estimate of monolayer cloud proportion in the tropics while underestimating this proportion at midlatitudes (see the gray line in Fig. 10b). This tendency of overestimation of multilayer cases at midlatitudes is known for the PH algorithm (Wind et al. 2010; Platnick et al. 2015). For cloudy scenes over land, not shown here, the estimated climatologies exhibit the same feature: POLDER gets the global feature with an underestimation of monolayer proportion; MODIS

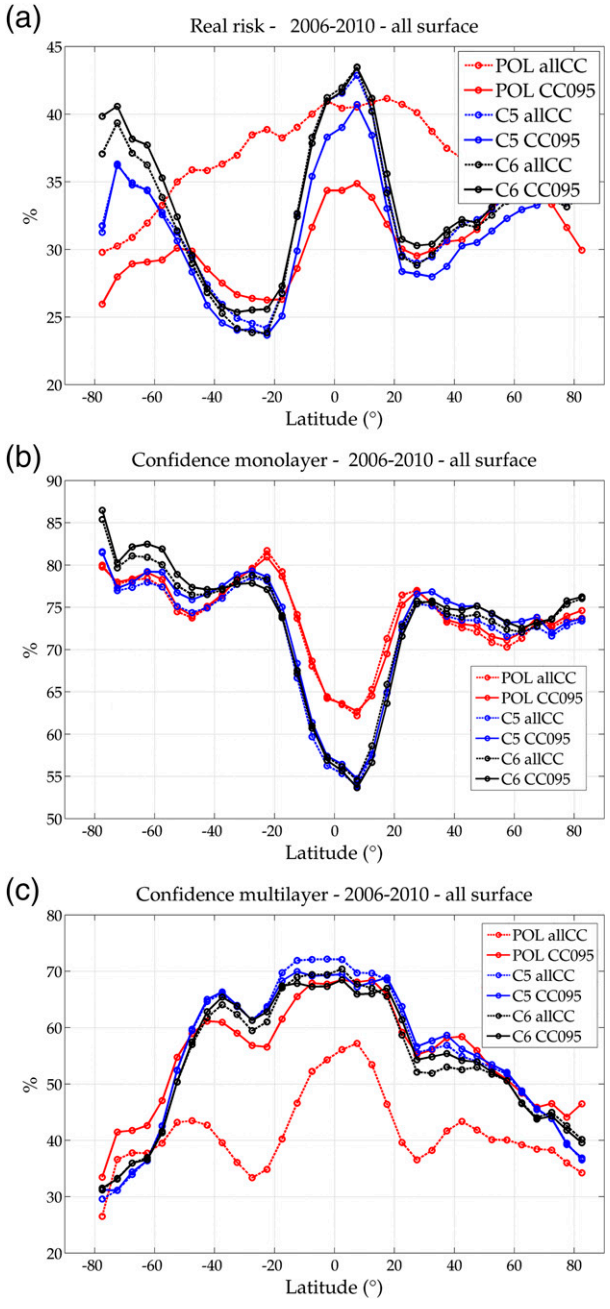

FIG. 9. Zonal variations of (a) the real risk and of the confidences in (b) the monolayer classification and (c) the multilayer classification. Risk and confidences are for POLDER (POL) and MODIS C5 and C6 classifications for all surfaces over the period 2006–10.

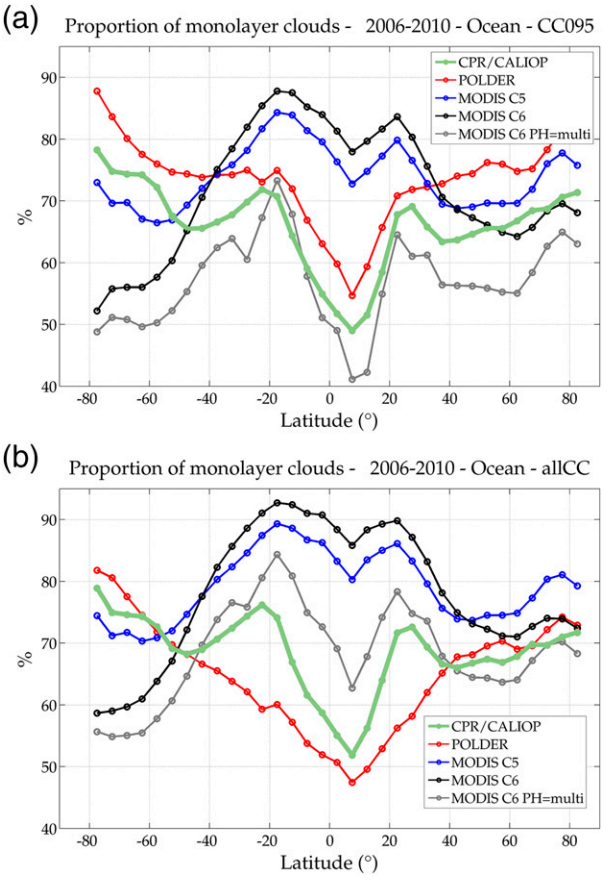

FIG. 10. Zonal proportion of monolayered clouds over 2006–10 from *CloudSat*/CALIOP, POLDER, and MODIS for (a) clouds over ocean with CC > 0.95 and $\tau \geq 5$, and (b) all clouds.

C5 and C6 overestimate largely this proportion in the tropics.

It is interesting to observe the sensitivity of the retrieved climatologies to the amount of cloud cover, as already done for the risk and confidence in the classification. Figure 10b shows the corresponding proportion of monolayer clouds for all cloud cover over the time period. The "reference" climatology shows a global increase of this fraction, as already noted in Fig. 1a, and this tendency is verified for climatologies inferred from MODIS data. It is the contrary for POLDER, which shows a global decrease of it. POLDER actually classifies some fractional cloud covers with low optical depth as multilayer scenes. For these scenes, the angular contrast in the observation might increase, interpreted in our algorithm as an effect of multiple cloud layers. It is consistent with the observed increase of the risk (see in Fig. 9a) and the decrease of the multilayer confidence (see Fig. 9c) from CC095 to allCC. For MODIS, while their corresponding risk and confidence varies weakly with CC, their inferred climatologies happen to be more sensitive to it.

6. Conclusions

In this paper, we present the definition of a cloud multilayer flag based on POLDER–*PARASOL* measurements. This flag allows identifying the multilayer

character of cloudy situations. To obtain this new cloud parameter, we first distinguished between monolayered and multilayered cloud scenes from the measurements of the A-Train active sensors when there was a coincidence of the measurements. This showed us the sensitivity of POLDER level-2 parameters to the mono–multilayer character of cloud situations, hence containing information about this character. We built a decision tree that performs a statistical classification of cloud scenes through a series of tests on the POLDER parameters. The tests that are retained bring the most information about the studied character for successive populations of cloud scenes. The attribute that distinguishes the most between the two types of situations and that stands for the first node of the tree is a threshold (22.5 hPa) on the angular standard deviation of the oxygen pressure $\sigma_{P_{O_2}}$, hence exploiting the multidirectional character of POLDER measurements. This result has been validated with a second independent technique (ROC curve). The multilayer flag that is obtained is the final result of the tree's statistical classification and represents directly a confidence in the mono–multilayer character of each cloud scene. An analysis of the tree's classification with a concern about its physical sense shows that the application of a general and rigorous statistical classification method, based on rightly chosen attributes, does not produce physical inconsistency.

The POLDER multilayer flag MLF_{pol} takes 20 discrete values between 0 and 100. Values closest to zero indicate a higher confidence in the monolayer character and closest to 100 a higher confidence in the multilayer character. This indicator can be used either as a confidence in the mono–multilayer character of a cloudy scene or, used with a threshold, can lead to a binary index to distinguish between monolayer and multilayer clouds. A study of the real risk of misclassification as a function of the threshold shows that the risk is minimized with a threshold of 44. With this rule for a binary distinction, and for cloud layers with a POLDER cloud cover higher than 0.95 and cloud optical depth higher than 5—denoted as CC095—the confidence in the estimated monolayer (multilayer) character of the scene is 74.0% (58.2%) over the period 2006–10. The mean risk to misidentify a cloudy situation over all latitudes is 30.5%, ranging between 29% and 34% over 5 yr. The risk is higher over land than over ocean. The risk is maximum in the tropics, and it comes from a decrease in the confidence in the monolayer classification. It might be due to the high value of optical depth of high cloud layers above lower ones. A quantitative evaluation of the multilayer classification from MODIS C5 and C6 shows quite similar results, which is remarkable considering that the principles of the two classifications are very different. MODIS risks of misclassification are slightly higher than the risks of POLDER. However, POLDER risk and multilayer confidence are more sensitive to the type of cloud cover, and the performance of the POLDER classification decreases significantly when cloud optical thickness is lower than 5, contrary to MODIS over ocean.

Finally, as a last evaluation of the POLDER multilayer classification, we studied the zonal climatology of monolayered and multilayered clouds as inferred from the passive sensors POLDER and compared with the reference climatology from CPR/CALIOP and MODIS measurements. For the cloud population CC095, POLDER provides a quite right feature of this climatology, with a minimum fraction of monolayer cases in the tropics and a maximum out of it. However, POLDER overestimates globally by 6% the cloud monolayer proportion. This is certainly partly caused by the non-discernment of thin layers of high ice clouds above lower cloud layers. Another important aspect of POLDER classification is that POLDER interprets some monolayer optically thin layers as multilayered cases. The MODIS algorithms, on the contrary, provide, with precaution taken, a correct proportion of monolayered clouds at midlatitudes. However, they overestimate significantly the proportion of monolayer clouds in the tropics.

These results demonstrate the potential and complexity for passive sensors to identify cloud scenes as monolayered or multilayered. POLDER measurements are sensitive to the multilayer character of cloud scenes, and the resulting POLDER multilayer classification, obtained from a very general decision tree approach, comes with interesting performances in terms of confidences in the classification, risk of misclassification, and inferred climatology, both inside and outside of the tropics. One of the perspectives of this study is to pursue the analysis of the classification's performance. One must further analyze which cloud monolayer and multilayer scenes are well identified by POLDER and which are not. Then, we aim to analyze again the performance and significance of other POLDER cloud parameters in view of this new information about the inferred cloud vertical structure. The combined use of the two passive sensors POLDER and MODIS should also be certainly considered, as their capacities for classifying cloud scenes might well be complementary in different situations and improve the possible description of the multilayer character of cloud scenes with passive sensors.

Acknowledgments. This study has been financed through grants from the CNES and from the region Nord-Pas-De-Calais. We are grateful to the ICARE data center (http://www.icare.univ-lille1.fr/) for providing easy access to *CALIPSO*-collocated *PARASOL*, *CloudSat*, and MODIS data (MULTI_SENSOR data project) as well as computing resources.

REFERENCES

Andrews, T., J. M. Gregory, M. J. Webb, and K. E. Taylor, 2012: Forcing, feedbacks and climate sensitivity in CMIP5 coupled atmosphere–ocean climate models. *Geophys. Res. Lett.*, **39**, L09712, doi:10.1029/2012GL051607.

Baum, B. A., and J. D. Spinhirne, 2000: Remote sensing of cloud properties using MODIS airborne simulator imagery during SUCCESS: 3. Cloud overlap. *J. Geophys. Res.*, **105**, 11 793–11 804, doi:10.1029/1999JD901091.

——, and Coauthors, 1995: Satellite remote sensing of multiple cloud layers. *J. Atmos. Sci.*, **52**, 4210–4230, doi:10.1175/1520-0469(1995)052<4210:SRSOMC>2.0.CO;2.

Bloom, S., and Coauthors, 2005: Documentation and validation of the Goddard Earth Observing System (GEOS) data assimilation system—Version 4. NASA Tech. Memo. NASA/TM-2005-104606, 165 pp.

Bony, S., and J.-L. Dufresne, 2005: Marine boundary layer clouds at the heart of tropical cloud feedback uncertainties in climate models. *Geophys. Res. Lett.*, **32**, L20806, doi:10.1029/2005GL023851.

Bréon, F.-M., and M. Doutriaux-Boucher, 2005: A comparison of cloud droplet radii measured from space. *IEEE Trans. Geosci. Remote Sens.*, **43**, 1796–1805, doi:10.1109/TGRS.2005.852838.

Buriez, J. C., and Coauthors, 1997: Cloud detection and derivation of cloud properties from POLDER. *Int. J. Remote Sens.*, **18**, 2785–2813, doi:10.1080/014311697217332.

Chang, F.-L., and Z. Li, 2005: A new method for detection of cirrus overlapping water clouds and determination of their optical properties. *J. Atmos. Sci.*, **62**, 3993–4009, doi:10.1175/JAS3578.1.

Chepfer, H., V. Noel, D. Winker, and M. Chiriaco, 2014: Where and when will we observe cloud changes due to climate warming? *Geophys. Res. Lett.*, **41**, 8387–8395, doi:10.1002/2014GL061792.

Christensen, M. W., G. G. Carrió, G. L. Stephens, and W. R. Cotton, 2013: Radiative impacts of free-tropospheric clouds on the properties of marine stratocumulus. *J. Atmos. Sci.*, **70**, 3102–3118, doi:10.1175/JAS-D-12-0287.1.

Cornuéjols, A., and L. Miclet, 2010: *Apprentissage Artificiel.* 2nd ed. Eyrolles, 804 pp.

Cover, T. M., and J. A. Thomas, 1991: *Elements of Information Theory.* Wiley, 542 pp.

Desmons, M., N. Ferlay, F. Parol, L. Mcharek, and C. Vanbauce, 2013: Improved information about the vertical location and extent of monolayer clouds from POLDER3 measurements in the oxygen A-band. *Atmos. Meas. Tech.*, **6**, 2221–2238, doi:10.5194/amt-6-2221-2013.

Fawcett, T., and F. Provost, 1996: Combining data mining and machine learning for effective user profiling. *Proc. Second Int. Conf. on Knowledge Discovery and Data Mining*, Portland, OR, Association for the Advancement of Artificial Intelligence, 8–13.

Ferlay, N., and Coauthors, 2010: Toward new inferences about cloud structures from multidirectional measurements in the oxygen A band: Middle-of-cloud pressure and cloud geometrical thickness from POLDER-3/*PARASOL*. *J. Appl. Meteor. Climatol.*, **49**, 2492–2507, doi:10.1175/2010JAMC2550.1.

Gabriel, P., H. W. Barker, D. O'Brien, N. Ferlay, and G. L. Stephens, 2009: Statistical approaches to error identification for plane-parallel retrievals of optical and microphysical properties of three-dimensional clouds: Bayesian inference. *J. Geophys. Res.*, **114**, D06207, doi:10.1029/2008JD011005.

Goloub, P., M. Herman, H. Chepfer, J. Riedi, G. Brogniez, P. Couvert, and G. Séze, 2000: Cloud thermodynamical phase classification from the POLDER spaceborne instrument. *J. Geophys. Res.*, **105**, 14 747–14 759, doi:10.1029/1999JD901183.

Green, D. M., and J. A. Swets, 1966: *Signal Detection Theory and Psychophysics.* John Wiley and Sons, 455 pp.

Hahn, C. J., S. G. Warren, J. London, R. M. Chervin, and R. Jenne, 1990a: Atlas of simultaneous occurrence of different cloud types over land. NCAR Tech. Note NCAR/TN-241+STR, 218 pp.

——, ——, ——, ——, and ——, 1990b: Atlas of simultaneous occurrence of different cloud types over the ocean. NCAR Tech. Note NCAR/TN-201+STR, 212 pp.

Hand, D. J, and R. J. Till, 2001: A simple generalisation of the area under the ROC curve to multiple class classification problems. *Mach. Learn.*, **45**, 171–186, doi:10.1023/A:1010920819831.

Hanley, J. A., and B. J. McNeil, 1982: The meaning and use of the area under a receiver operating characteristic (ROC) curve. *Radiology*, **143**, 29–36, doi:10.1148/radiology.143.1.7063747.

Heidinger, A. K., and M. J. Pavolonis, 2005: Global daytime distribution of overlapping cirrus cloud from NOAA's Advanced Very High Resolution Radiometer. *J. Climate*, **18**, 4772–4784, doi:10.1175/JCLI3535.1.

Jin, Y., and W. B. Rossow, 1997: Detection of cirrus overlapping low-level clouds. *J. Geophys. Res.*, **102**, 1727–1737, doi:10.1029/96JD02996.

Joiner, J., A. P. Vasilkov, P. K. Bhartia, G. Wind, S. Platnick, and W. P. Menzel, 2010: Detection of multi-layer and vertically-extended clouds using A-train sensors. *Atmos. Meas. Tech.*, **3**, 233–247, doi:10.5194/amt-3-233-2010.

King, M. D., and Coauthors, 2003: Cloud and aerosol properties, precipitable water, and profiles of temperature and water vapor from MODIS. *IEEE Trans. Geosci. Remote Sens.*, **41**, 442–458, doi:10.1109/TGRS.2002.808226.

Mace, G. G., Q. Zhang, M. Vaughan, R. Marchand, G. Stephens, C. Trepte, and D. Winker, 2009: A description of hydrometeor layer occurrence statistics derived from the first year of merged *CloudSat* and *CALIPSO* data. *J. Geophys. Res.*, **114**, D00A26, doi:10.1029/2007JD009755.

Mason, S. J., and N. E. Graham, 1999: Conditional probabilities, relative operating characteristics, and relative operating levels. *Wea. Forecasting*, **14**, 713–725, doi:10.1175/1520-0434(1999)014<0713:CPROCA>2.0.CO;2.

Menzel, W. P., and Coauthors, 2008: MODIS global cloud-top pressure and amount estimation: Algorithm description and results. *J. Appl. Meteor. Climatol.*, **47**, 1175–1198, doi:10.1175/2007JAMC1705.1.

Nasiri, S. L., and B. A. Baum, 2004: Daytime multilayered cloud detection using multispectral imager data. *J. Atmos. Oceanic Technol.*, **21**, 1145–1155, doi:10.1175/1520-0426(2004)021<1145:DMCDUM>2.0.CO;2.

Olson, R. H., 1965: On the use of Bayes' theorem in estimating false alarm rates. *Mon. Wea. Rev.*, **93**, 557–558, doi:10.1175/1520-0493(1965)093<0557:OTUOBT>2.3.CO;2.

Pavolonis, M. J., and A. K. Heidinger, 2004: Daytime cloud overlap detection from AVHRR and VIIRS. *J. Appl. Meteor.*, **43**, 762–778, doi:10.1175/2099.1.

Platnick, S., 2000: Vertical photon transport in cloud remote sensing problems. *J. Geophys. Res.*, **105**, 22 919–22 935, doi:10.1029/2000JD900333.

——, M. D. King, S. A. Ackerman, W. P. Menzel, B. A. Baum, J. C. Riédi, and R. A. Frey, 2003: The MODIS cloud products: Algorithms and examples from *Terra*. *IEEE Trans. Geosci. Remote Sens.*, **41**, 459–473, doi:10.1109/TGRS.2002.808301.

——, and Coauthors, 2015: MODIS cloud optical properties: User guide for the collection 6 level-2 MOD06/MYD06 product and associated level-3 datasets. NASA Tech. Rep., 141 pp. [Available online at https://modis-atmos.gsfc.nasa.gov/_docs/C6MOD06OPUserGuide.pdf.]

Riedi, J., and Coauthors, 2010: Cloud thermodynamic phase inferred from merged POLDER and MODIS data. *Atmos. Chem. Phys.*, **10**, 11 851–11 865, doi:10.5194/acp-10-11851-2010.

Shannon, C. E., and W. Weaver, 1949: *The Mathematical Theory of Communication.* University of Illinois Press, 125 pp.

Sheu, R.-S., J. A. Curry, and G. Liu, 1997: Vertical stratification of tropical cloud properties as determined from satellite. *J. Geophys. Res.*, **102**, 4231–4245, doi:10.1029/96JD02867.

Sourdeval, O., L. C.-Labonnote, A. J. Baran, and G. Brogniez, 2015: A methodology for simultaneous retrieval of ice and liquid water cloud properties. Part I: Information content and case study. *Quart. J. Roy. Meteor. Soc.*, **141**, 870–882, doi:10.1002/qj.2405.

Stephens, G. L., and Coauthors, 2002: The *CloudSat* mission and the A-Train: A new dimension of space-based observations of clouds and precipitation. *Bull. Amer. Meteor. Soc.*, **83**, 1771–1790, doi:10.1175/BAMS-83-12-1771.

——, and Coauthors, 2008: *CloudSat* mission: Performance and early science after the first year of operation. *J. Geophys. Res.*, **113**, D00A18, doi:10.1029/2008JD009982.

Swets, J. A., 1988: Measuring the accuracy of diagnostic systems. *Science*, **240**, 1285–1293, doi:10.1126/science.3287615.

Vanbauce, C., J. C. Buriez, F. Parol, B. Bonnel, G. Sèze, and P. Couvert, 1998: Apparent pressure derived from ADEOS-POLDER observations in the oxygen A-band over ocean. *Geophys. Res. Lett.*, **25**, 3159–3162, doi:10.1029/98GL02324.

——, B. Cadet, and R. T. Marchand, 2003: Comparison of POLDER apparent and corrected oxygen pressure to ARM/MMCR cloud boundary pressures. *Geophys. Res. Lett.*, **30**, 1212, doi:10.1029/2002GL016449.

Vial, J., J.-L. Dufresne, and S. Bony, 2013: On the interpretation of inter-model spread in CMIP5 climate sensitivity estimates. *Climate Dyn.*, **41**, 3339–3362, doi:10.1007/s00382-013-1725-9.

Wang, J., W. B. Rossow, and Y. Zhang, 2000: Cloud vertical structure and its variations from a 20-yr global rawinsonde dataset. *J. Climate*, **13**, 3041–3056, doi:10.1175/1520-0442(2000)013<3041:CVSAIV>2.0.CO;2.

Warren, S., R. Eastman, and C. J. Hahn, 2014: Clouds and fog: Climatology. *Encyclopedia of Atmospheric Sciences*, 2nd ed. G. R. North, J. Pyle, and F. Zhang, Eds., Oxford University Press, 161–169.

Watts, P. D., R. Bennartz, and F. Fell, 2011: Retrieval of two-layer cloud properties from multispectral observations using optimal estimation. *J. Geophys. Res.*, **116**, D16203, doi:10.1029/2011JD015883.

Wilks, D. S., 1995: *Statistical Methods in the Atmospheric Sciences: An Introduction.* Academic Press, 467 pp.

Wind, G., S. Platnick, M. D. King, P. A. Hubanks, M. J. Pavolonis, A. K. Heidinger, P. Yang, and B. A. Baum, 2010: Multilayer cloud detection with the MODIS near-infrared water vapor absorption band. *J. Appl. Meteor. Climatol.*, **49**, 2315–2333, doi:10.1175/2010JAMC2364.1.

Winker, D. M., W. H. Hunt, and M. J. McGill, 2007: Initial performance assessment of CALIOP. *Geophys. Res. Lett.*, **34**, L19803, doi:10.1029/2007GL030135.

——, and Coauthors, 2010: The *CALIPSO* mission: A global 3D view of aerosols and clouds. *Bull. Amer. Meteor. Soc.*, **91**, 1211–1229, doi:10.1175/2010BAMS3009.1.

Yao, Z., Z. Han, Z. Zhao, L. Lin, and X. Fan, 2010: Synergetic use of POLDER and MODIS for multilayered cloud identification. *Remote Sens. Environ.*, **114**, 1910–1923, doi:10.1016/j.rse.2010.03.014.

Yuan, T., and L. Oreopoulos, 2013: On the global character of overlap between low and high clouds. *Geophys. Res. Lett.*, **40**, 5320–5326, doi:10.1002/grl.50871.